6-16-2008

Oxidation Resistance Studies of CrAlN Coatings on 430 Stainless Steel

Kurtis Wickey
Western Michigan University, kurtis.wickey@gmail.com

WESTERN MICHIGAN UNIVERSITY

The Carl and Winifred Lee Honors College

THE CARL AND WINIFRED LEE HONORS COLLEGE

CERTIFICATE OF ORAL DEFENSE OF HONORS THESIS

Kurtis Wickey, having been admitted to the Carl and Winifred Lee Honors College in Fall 2004, successfully presented the Lee Honors College Thesis on June 16, 2008.

The title of the project is:

Oxidation Resistance Studies of CrAlN Coatings on 430 Stainless Steel

Dr. Asghar Kayani, Physics

Dr. Clement Burns, Physics

Dr. Lisa Paulius, Physics

1903 W. Michigan Ave., Kalamazoo, MI 49008-5244
PHONE: (269) 387-3230 FAX: (269) 387-3903

Oxidation Resistance studies of CrAlN coatings on 430 Stainless Steel

A dissertation presented to

the faculty of

the College of Arts and Sciences of Western Michigan University

In partial fulfillment

of the requirements for the

Lee Honor's College

Kurtis Wickey

June 2008

I would like to dedicate this thesis to my grandparents and their dream of education for their grandchildren

Acknowledgements

I would like to extend my thanks to my supervisor Dr Asghar N. Kayani for the invaluable guidance that he gave me during my project and for editing of this thesis. He patiently answered all of my countless questions.

I wish to thank the committee members, Dr. Clement Burns, Dr. Lisa Paulius and Dr. Asghar Kayani (in alphabetic order), for their thoughtful comments.

A work like this cannot be carried out alone. You need support and help of others. I am grateful to the tireless efforts of Mr. Benjamin Guadio (Network engineer), Mr. Allen Kern, (Accelerator Engineer), Mr. Rick Welch (Manager machine shop), and in keeping the accelerator and other support equipment in good working order.

My thanks to my lab members, Elias Garratt, Andrew Moore and Manjula Nandasiri for their help and useful discussions. There are many from behind the scenes whom have encouraged and supported my work, and I wish to thank them all.

Abstract

The requirements of low cost and high-temperature corrosion resistance for interconnect plates in solid oxide fuel cell stacks has directed attention to the use of metal plates with oxidation resistant coatings. We have investigated the performance of stainless steel plates with homogenous coatings of CrAlN. The coatings were deposited using RF magnetron sputtering, with Ar as a sputtering gas and N as reactive gas. The Cr/Al composition ratio in the coatings was varied in a combinatorial approach. The coatings were subsequently annealed in air for up to 25 hours at 800 ^{o}C. The composition of the coated plates and the rate of oxidation were characterized using Rutherford backscattering (RBS) and nuclear reaction analysis (NRA). From our results, we conclude that Al rich coatings are more susceptible to oxidation than Cr rich coatings and a Cr/Al ratio of 0.9 offers the best resistant to oxidation.

Table of Contents

Chapter One

1. Introduction

Due to the rising demand for energy, especially from developing nations, and the complex issue of global warming, there is much interest in alternatives to fossil fuels. One of these alternatives is using hydrogen as a fuel. The main benefits of hydrogen is that its product is clean (water) and that it can be produced domestically thus lessening foreign dependence. Hydrogen can be utilized as a fuel in electrochemical devices called fuel cells. Current fuel cells have a higher efficiency than conventional power production methods since the fuel cells are not subject to the Carnot efficiency limit. The main barrier to a hydrogen economy is storage and cost of the fuel cells.

A fuel cell is by definition a device that generates electricity via a chemical reaction. Fuel cells are simple devices, containing no moving parts, whose make-up consists of only four functional component elements: cathode, electrolyte, anode and interconnect. The electrolyte is sandwiched between the cathode and anode, and consists of a thin, dense, ion conducting material. The cathode and anode are porous, ionic and electronic

conducting materials. Porosity in these materials allows the gases to reach the interface with the electrolyte. In solid oxide fuel cell (SOFC), as shown is fig. 1, oxygen in air, from the cathode side ionizes and passes through the electrolyte and combines with the hydrogen on the anode side to form water. As a result of this reaction two electrons flow in the circuit that constitutes electric current.

The solid oxide fuel cell (SOFC) has been an object of research for many years. Since the SOFC is a solid-state device, it has many advantages from the point of view of mechanical simplicity. The SOFC is also very flexible in the way it can be made, and its possible size. It therefore has scope for a wide variety of applications. SOFCs can be made from a range of different materials, with different operating temperatures, from about 650°C to 1000°C.

Although the operating concept of SOFCs is rather simple, the selection of materials for the individual components presents enormous challenges. Each material must have the electrical properties required to perform its function in the cell. There must be enough chemical and structural stability to endure fabrication and operation at high temperatures. In order to achieve sufficiently high current densities through the electrolyte and power outputs, the fuel cell operating temperatures must be in the range of ~700-1000 °C.

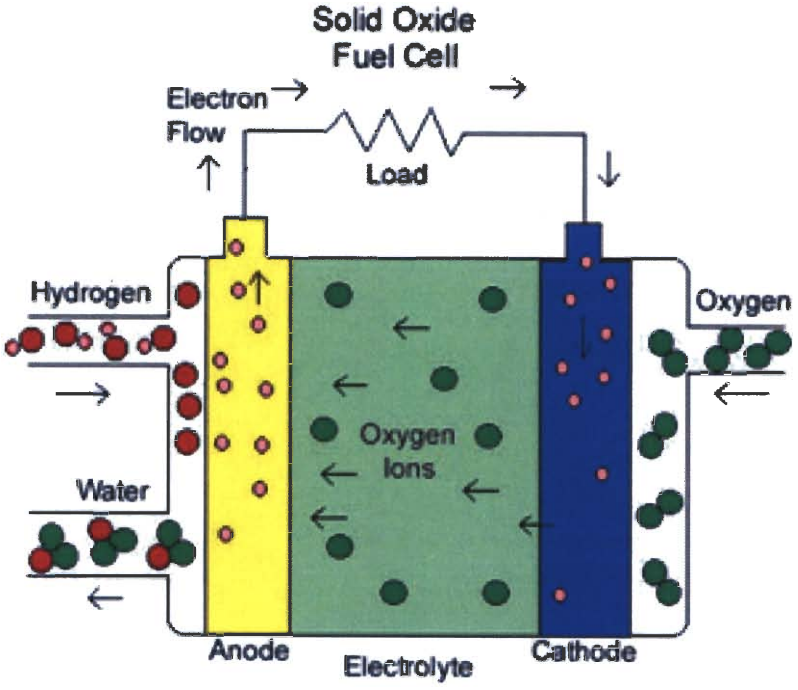

Fig. 1: A simple example of SOFC hydrogen fuel cell [5]

Until recently SOFCs have all been based on an electrolyte of zirconia stabilized with the addition of a small percentage of yttria oxide (Y_2O_3). Above a temperature of about 800°C, zirconia becomes a conductor of oxygen ions and the typical zirconia-based SOFC operates between 800 and 1100°C. This is the highest operating temperature of all fuel cells, which presents both challenges for the construction and durability, and also opportunities. For example, in combined cycle (bottoming cycle) there are applications where SOFC can be combined together with a steam turbine.

The anode of the SOFC is usually a zirconia cermet (an intimate mixture of ceramic and metal). The metallic component is nickel, chosen amongst other things because of its high electronic conductivity and stability under chemically reducing conditions. The presence of nickel can be used to advantage as an internal reforming catalyst and it is possible to carry out internal reforming in the SOFC directly on the anode [1].

The material for the cathode has been something of a challenge. In the early days of development noble metals were used, but have fallen out of favor on cost grounds. Most SOFC cathodes are now made from electronically conducting oxides or mixed electronically conducting and ion-conducting ceramics. The most common cathode material of the later type is strontium-doped lanthanum manganite.As mentioned previously, the formation of water is the chemical reaction used in hydrogen fuel cells. In chemical notation it is written as [5]:

$$2H_2 + 2O^{2-} \rightarrow 2H_2O + 2e- \qquad (1)$$

At standard temperature and pressure the energy that can be freed from this reaction (called the Gibb's free energy change notated ΔG) is about -237.2 kJ/mole [2].

Using chemical potentials and half reactions at the interfaces, it can be shown that the Gibb's free energy change for any temperature and pressure can be calculated by [3]:

$$\Delta G = \Delta G^0 + RT \ln\left(\frac{p_{H_2O}}{p_{H_2} p_{O_2}^{1/2}}\right) \qquad (2)$$

Where ΔG^0 is the change at standard temperature and pressure mentioned previously, and p subscripts refers to the partial pressures of the respective gasses. R and T stand for the usual thermodynamic entities. This ΔG is related to the fuel cell potential. The cell potential is related to ΔG using the maximum work theorem by [4]:

$$\Delta G = -nF\Delta E \qquad (3)$$

Where n is the number of electrons transferred in the chemical reaction (for the hydrogen fuel cell it is 2, refer to equation 1), F is Faraday's constant, and ΔE is the potential across the cell. Combining equations 2 and 3, we have the relation for the reversible cell potential [3]:

$$E_{rev} = \Delta E^0 + \frac{RT}{2F} \ln\left(\frac{p_{H_2} p_{O_2}^{1/2}}{p_{H_2O}}\right) \qquad (4)$$

For a SOFC operating at 1000 °C, this is on the order of 1 volt [5].

For high voltage outputs, cells are connected together in series. The "interconnect" is the means by which connection is achieved between neighboring fuel cells. In planar fuel cell terminology this is the bipolar plate. Metals can be used as the interconnect, but these tend to be expensive "inconel" type stainless steels, particularly for stacks that need to operate at 800 to 1000°C. Metal interconnects also tend to form oxide coatings, which can limit their electrical conductivity and act as a barrier to mass transport.

The high operating temperature of the cell combined with severe operating environments necessitates that the interconnect connecting the individual fuel cells in series must meet the most stringent requirements of all of the cell components: electrical

conductivity, no porosity (to avoid mixing of fuel and oxygen), thermal expansion compatibility, and inertness with respect to the other fuel cell components. Any reduction in component costs, directly translates into improved energy affordability. The strong economic incentive is to use traditional metals for interconnects, such as stainless steel. But at such high temperatures and under an oxidizing atmosphere, stainless steel becomes oxidized and the cell performance is lost. Interconnect deterioration is one of the biggest problems impeding the commercialization of fuel cells.

The operational requirements of high ionic conductivity and good catalytic performance in the fuel cell must be balanced against the practical requirements of low cost and high-temperature corrosion resistance for components in the fuel cell stack [6]. The interconnect, must not only retain low electrical resistivity throughout the operating lifetime of the fuel cell, but must also have good surface stability and compatibility with thermal expansion properties of the materials in the stack. Doped $LaCrO_3$ plates have worked well for cells operating at 1000°C, but suffer from high cost as well as difficulties in fabrication. The recent trend towards lower operating temperatures (500–750°C) may enable the use of more cost-effective materials for the interconnect. A thorough evaluation of several heat-resistant alloys with a variety of compositions led to the conclusion that it would be difficult for most traditional alloys to meet the materials requirements of long-term operation above 700°C [7].

Alloys of body centered cubic ferritic stainless steels appear to have thermal expansion coefficients that are well matched to other components in the stack. Moreover, metallic interconnects promise lower cost, higher strength, and higher thermal

conductivity than conventional interconnects. They can be employed if thinner and higher-conductivity solid electrolytes are used, allowing lower operating temperatures that suitable metals can withstand. Therefore, for improved oxidation resistance and electrical conductivity, either new alloys will be needed, or surface engineering of existing alloys will be required [7].

Proposed experimental research is to characterize the stainless steel coated coupons, deposited with CrAlN coatings with variable Cr/Al ratio. These samples are studied for the possible interconnect application. Oxidation resistances of these samples are analyzed using ion beam analysis techniques.

Chapter Two

2. Ion Beam Analysis

Rutherford Backscattering spectroscopy (RBS) and Nuclear Reaction Analysis (NRA) are two quantitative ion beam based techniques to study composition, structure and interface of the near surface region of the material.

Rutherford Backscattering uses elastic collisions between the target and incident atoms to determine the concentration of the target atom in the material. A silicon surface barrier detector placed at angle θ will detect the scattered particle with energy E_1. Knowing the initial energy of the incident particle, E_0, one can determine the mass of the target atom by using the conservation of momentum.

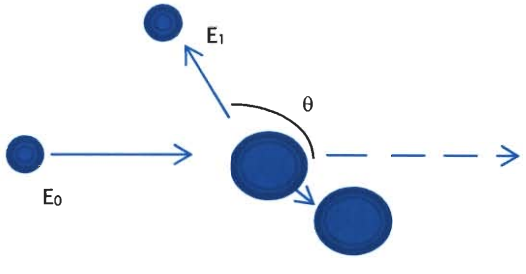

Fig. 1: The incident ion has energy E_0, when it scatters from the target nucleus at an angle θ, measured from the outgoing path, it has energy E_1

The kinematic factor, K, is defined as the ratio between the scattered particle's energy E_1 and the incident particle's energy E_0. Using the conservation of momentum, K can be

calculated for a particular scattering angle θ using the masses of the incident ion and the target atom [8]:

$$K = \left[\frac{\left(M_2^2 - M_1^2 \sin^2\theta\right)^{\frac{1}{2}} + M_1 \cos\theta}{M_1 + M_2} \right]^2 \qquad (1)$$

Where M_1 and M_2 are the masses of the incident and target particles respectively. There is a limit of how well RBS can resolve two target atoms of similar mass. This is due to the limited energy resolution of silicon surface barrier detectors and the difference between the kinematic factors of the two atoms. The energy separation ΔE of the particles scattered by two different atoms of mass difference ΔM at a fixed θ is given by [8]:

$$\Delta E = E_0 \left(\frac{dK}{dM_2} \right) \Delta M \qquad (2)$$

Where dK/dM_2 is the change in the kinematic factor due to the change in the target mass. Thus in fig 2, the energy separation of two heavier atoms of mass difference ΔM will be larger using a He beam than a H beam since the change in the kinematic factor for He is larger than for H.

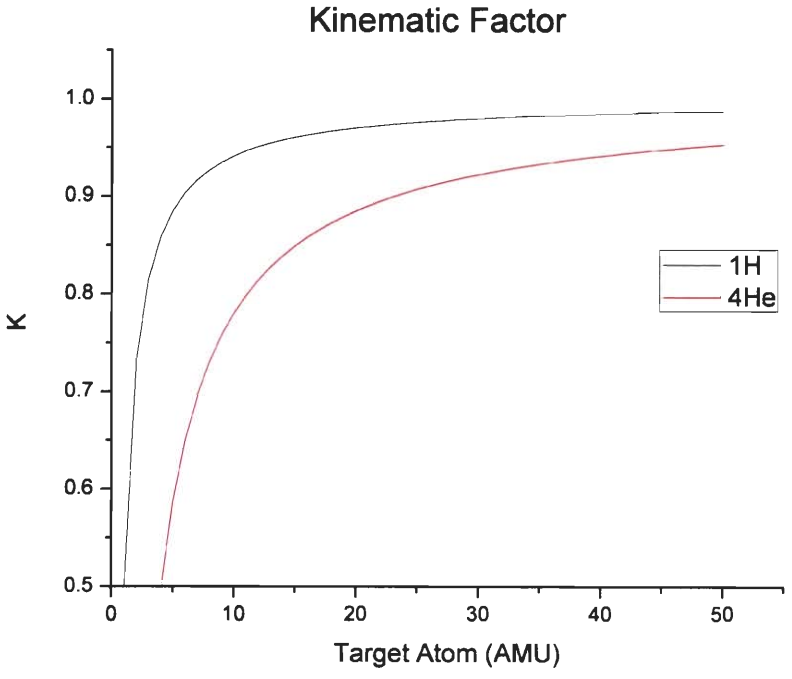

Fig. 2: A plot showing the Kinematic factor as the target mass changes. The scattering angle is 150 degrees. The incident ions are H and He

Since the detector has a minimum energy resolution, one can calculate the mass resolution, δM by using equation 3. Letting ΔE be equal to the minimum energy resolution δE of the detector and solving for ΔM [8]:

$$\delta M = \frac{\delta E}{E_0\left(\frac{dK}{dM_2}\right)} \tag{3}$$

This is the smallest mass resolution that can be resolved by the detector. Thus, RBS has good mass resolution for light elements, but poor mass resolution for heavy elements. For example, when He^{++} strikes light elements such as C or O, as shown in the figure 3, a significant fraction of the projectile's energy is transferred to the target atom and the energy recorded for that backscattering event is much lower than the energy of the beam. It is usually possible to resolve C from O, but difficult to resolve Cr from Fe and Au from Hg, even though all of these elements differ in mass by only about 4 Amu.

The cross-section is a measure of the probability that an incident particle will strike a target particle and scatter into a detector placed at an angle θ. It depends on both the scattering angle and the energy of the particle when it strikes the target.

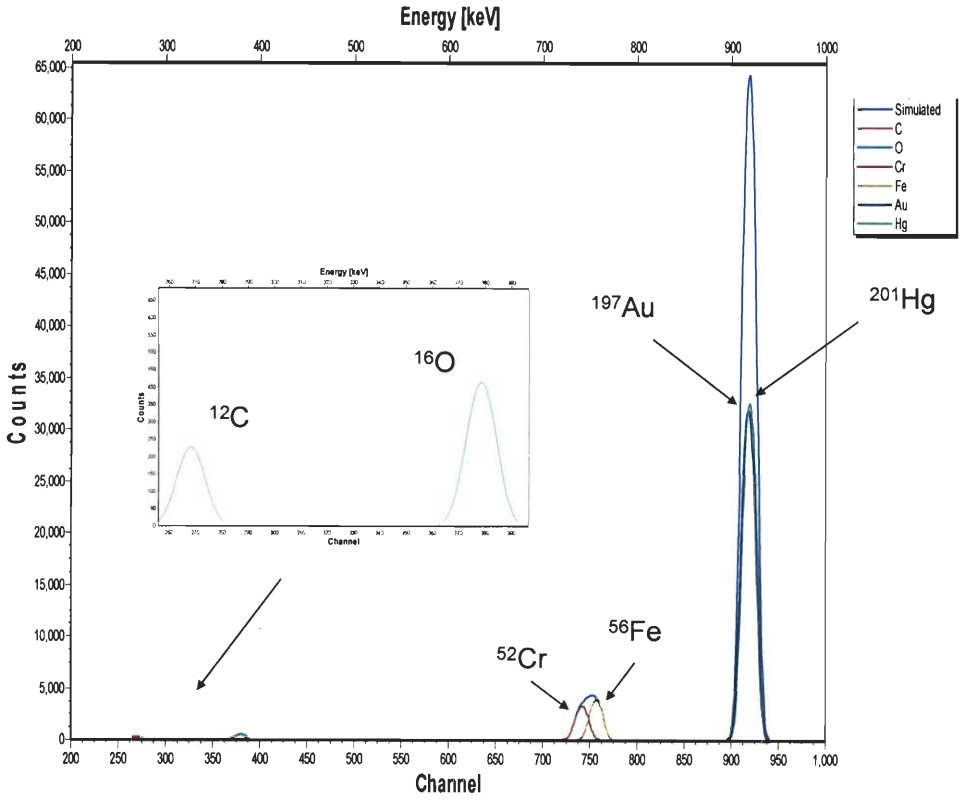

Fig. 3: Simulated spectra of 3 pairs of target atoms, all 4 Amu apart. The incident beam is ^{4}He at 1 MeV with a 150 degree scattering angle. Of these three pairs, only C and O are readily discernable (inset). Cr and Fe might be resolved with a better detector resolution, but Au and Hg are inseparable.

Assuming only a Coulomb interaction between the incident ion and the target particle and neglecting electron shielding [8]:

$$\sigma_R(E,\theta) = 4\left(\frac{Z_1 Z_2 e^2}{4E}\right)^2 \frac{\left[\left(M_2^2 - M_1^2 \sin^2\theta\right)^{\frac{1}{2}} + M_2 \cos\theta\right]^2}{M_2 \sin^4\theta\left(M_2^2 - M_1^2 \sin^2\theta\right)^{\frac{1}{2}}} \qquad (4)$$

Z_1 and Z_2 are the number of protons in the incident and target atoms respectively. E is the energy of the incident ion and e is the charge of an electron. If the target is thin, then E can be taken to be E_0 and the energy loss of the incident ion in the solid can be neglected. This leads to another limitation of the RBS method. It is more sensitive to heavy elements than for light elements, due to the larger scattering cross sections of the heavier elements. Therefore, RBS is particularly useful for obtaining concentration depth profiles for the heavier elements in the coating, but is somewhat limited in detecting the light elements such as O and N because of the quadratic dependence of the Rutherford cross section on the atomic number of the target atom.

Since we are working with CrAlN films on a stainless steel substrate, this is of special concern to us. Equation 4 shows the dependence of the cross-section on the target nucleus (Z_2). The cross-section of the Fe in the substrate is much larger than cross-section of either the O or N, therefore the scattered peaks from these elements sit on a large background, making it difficult for us to simulate. Figure 4 shows this phenomenon.

To overcome this limitation, we used Nuclear Reaction Analysis (NRA). A nuclear reaction takes place when the incident nuclei and target nuclei come so close to each other that nuclear forces start playing a role in the scattering process. Two types of

nuclear reactions can occur. In first type the nucleus of the target stays intact and the scattering probability is enhanced. At certain energies even resonant scattering can give rise to peaks that are signatures of the target nuclei. In the second type, the target nucleus becomes unstable and by releasing a particle that carries signature of the target nucleus, becomes a stable daughter nucleus. The spectral peaks resulting from this reaction typically sit on a very low or zero-background signal [8]. In both cases, scattering cross section is non-Rutherford. A limitation for NRA is that the reaction cross sections are generally known only for a few selected scattering angles, and thus may need to be measured using standard thin films of known stoichiometry.

Therefore, we used 3.0 MeV H^+ beam to take advantage of the non-Rutherford enhancement in the cross section of O and N at this energy and a beam of 1.1 MeV deuterium ions (D^+) to measure the O and N concentrations. The detected particles for these measurements were protons from the $^{14}N(d,p)^{15}N$ and $^{16}O(d,p)^{17}O$ reactions.

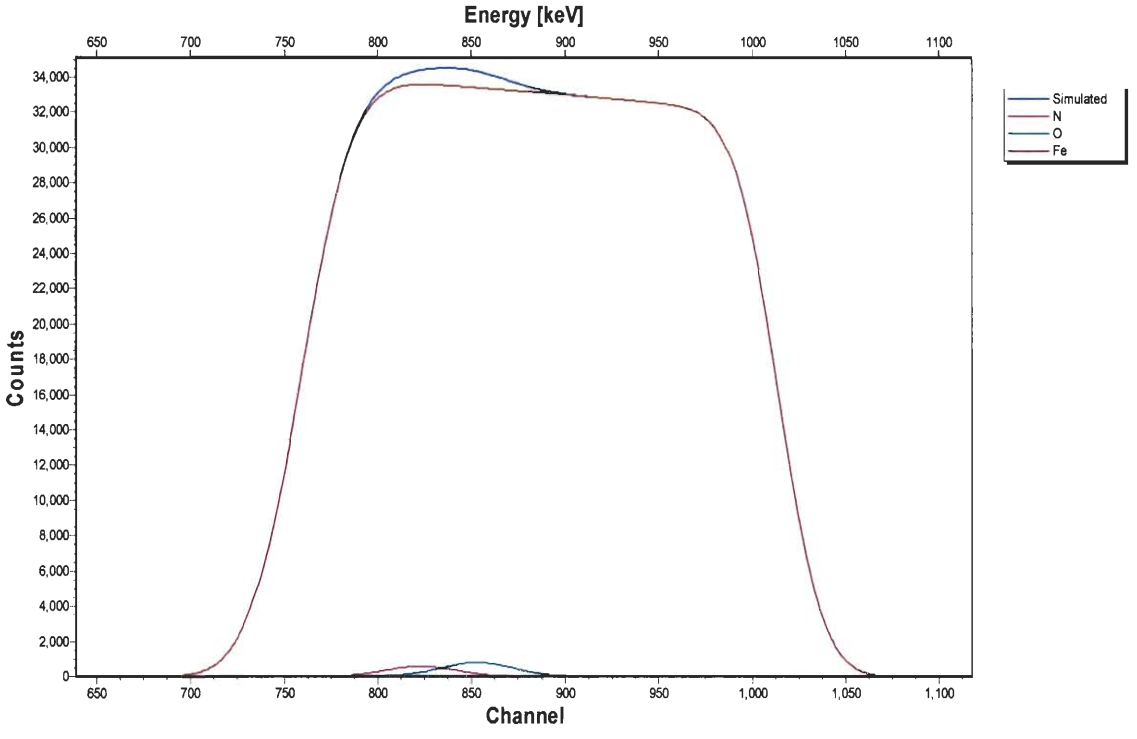

Fig 4: This is a simulated spectrum of a thin O/N film on top of Fe. The incident beam is H and the scattering angle is 165 degrees. The small peak on the left side of the Fe peak is the combined O and N peak. If this was experimental data, there wouldn't be anything useful to be obtained about the O/N ratio.

Chapter Three

Experiment

The use of coatings to improve oxidation resistance on metal alloys has been known for many years. We selected the Cr-Al-N system for study because it not only offers oxidation resistance at temperatures up to 900°C [9,10], but also offers a wear resistance typical of many metal nitrides [11].

Ion beam analysis was carried out on the samples obtained from Dr. Asghar Kayani. Detailed account of deposition process and the procedure adopted for the sample preparations can be found in the referenced article [12]. Kayani et al. used a 430 steel plate as sample substrate, of dimensions 15.2 x 10.6 cm. Sample coupons of dimension 1 x 2 cm were laser cut from the steel plate in such a way that these coupons were left attached to the plate with a small tab. This chamber used for the deposition process was fitted with three water-cooled balanced magnetron sputter heads mounted 120° apart on the horizontal plane and at an angle of 30° from the normal from the copper sample

holder, as shown in the figure 1. Each head had a shutter attached for soaking purposes. Chromium (99.999%) and aluminum (99.999%) metal targets were used to deposit coatings onto the stainless-steel sample plate at room temperature. Deposition time was 4 hours. The sample holder was held fixed so that a different Cr/Al ratio in the coating on the sample coupons was obtained. Depending upon their placement in the rectangular sample plate with respect to the Cr and Al gun positions as shown in figure 2, the coupons had different Cr/Al ratio. Five coupons, one from each corner plus the one in the center of the plate labeled A2, A10, C2, C10 and AC3 were analyzed by Kayani et al. [12]. The best oxidation performance was demonstrated by sample C2 which had a Cr/Al ratio of 0.9. For our study we selected samples labeled, A5, AC1, AC5 and C5.

Ion beam analysis of these samples was performed using a 6 MeV tandem Van de Graaff accelerator of the department of physics at Western Michigan University. Rutherford backscattering spectra (RBS) were recorded using 3.0 MeV beams of H^+ and 1.1 MeV D^+ ions, incident normal to the sample surface. Backscattered ions were collected using a silicon surface barrier detector at a scattering angle of 165°, with an exit angle of 15° as measured with respect to the sample's surface normal. A 3 MeV H^+ beam was used to determine the Cr/Al ratio for the samples and a 1.1 MeV D^+ beam was used to determine the N/O ratio using NRA. The four samples were placed in a vacuum chamber pumped down to 10^{-7} torr via an ion pump. The aluminum sample holder had three degrees of freedom, x, y and z-axis. Double sided, conducting carbon tape was used to restrain the samples on the sample holder. This arrangement is required to measure the total amount of charge bombarded on the sample. Current and charge on the sample was measured

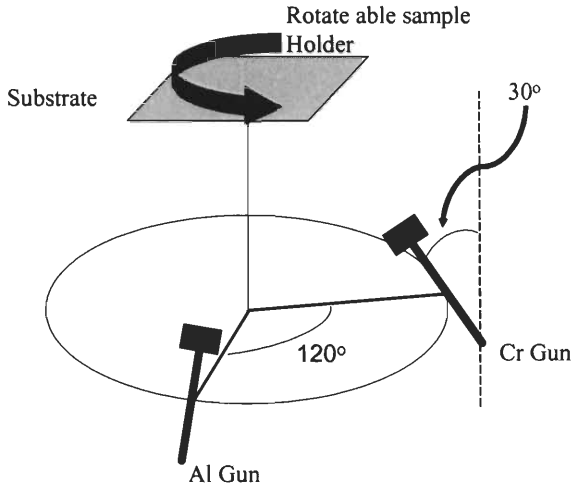

Fig 1: The setup of the sputtering process

A2	A1	AC1	C1	C2
A4	A3	AC2	C3	C4
A6	A5	AC3	C5	C6
A8	A7	AC4	C7	C8
A10	A9	AC5	C9	C10

Fig. 2: The sample plate. Samples A5,AC1,AC5,C5 were chosen for this study

using the ORTEC Model. 439 Digital Current Integrator. This instrument is designed to accurately measure dc currents or the average value of pulse currents produced by accelerator beams. It digitizes the input current by producing an output pulse for specific values of input charge. Output pulses of 10^{-10} coulombs each, were counted by a counter. These current pulses were converted into voltage pulses and amplified by a pre-amplifier. These voltage pulses were then further amplified by an additional amplifier These pulses or 'counts' were then read by a Multi-Channel Analyzer (MCA) which relates the voltage of the pulse to the energy of the detected particle. This relation is known as the calibration factor. The MCA was calibrated using a ^{241}Am source which emits alpha particles at 5.64 MeV. The resulting spectra are shown in figures 3 and 4.

In order to study the oxidation resistance characteristics of CrAlN films, samples were baked in a tube furnace at 800 °C in air. The oxidation periods for each sample were 1, 3, 5, 9, and 25 hours. Baking was carried out with a programmable temperature controller. Ramp times were programmed to allow for ramping of 5 °C a minute. Samples were removed from the oven after each oxidation period for ion beam analysis. Composition profiles for the samples (before and after oxidation) were generated using SIMNRA computer simulations of the spectra [13].

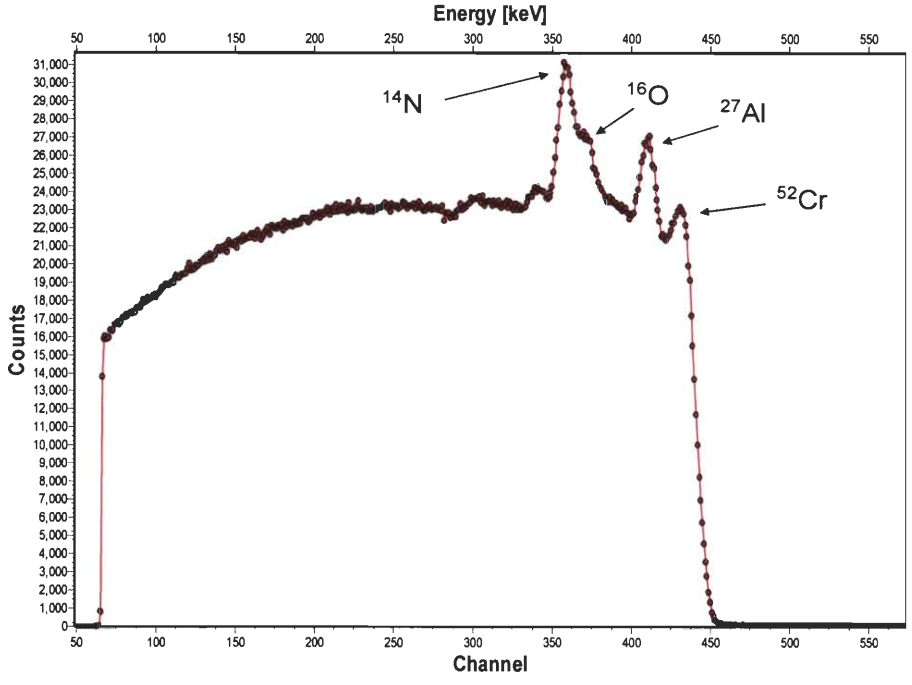

Fig. 3: 3 MeV H^+ spectra taken of sample C5 with a scattering angle of 165 degrees.

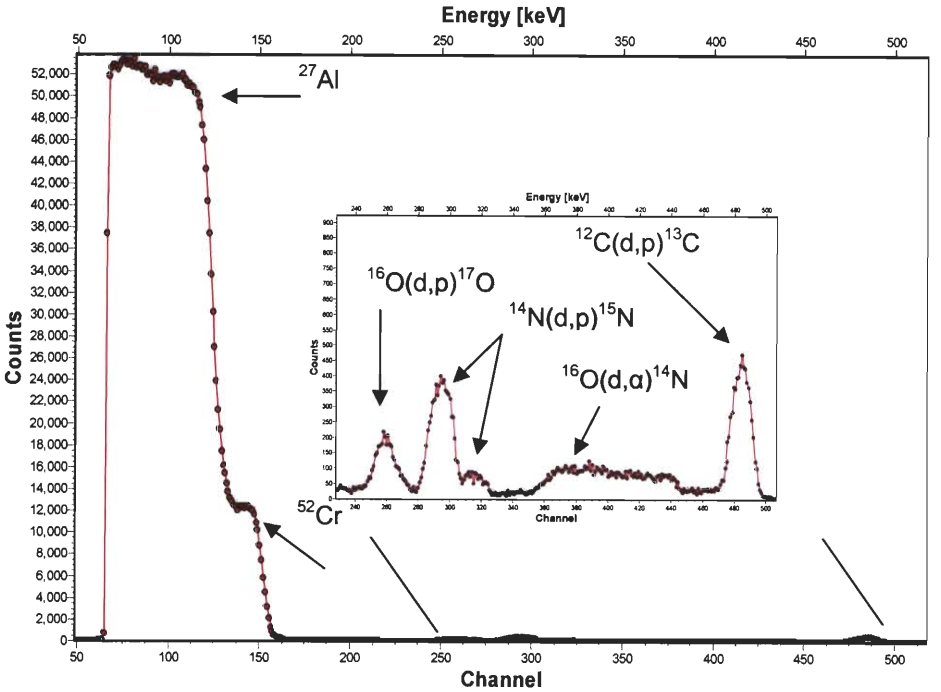

Fig. 4: 1.1 MeV D^+ base spectra taken of sample C5 with a scattering angle of 165 degrees. Inset shows the nuclear reactions sitting on the zero background. Magnification is about 5x.

Chapter Four

Results and discussion

After the samples were placed in the tube furnace for the intervals stated in the previous section, the following spectra were obtained. Figures 1, 2, 3 and 4 are the overlapped spectra of the samples, taken after each oxidation stage. ^{16}O and ^{14}N has several nuclear reactions with the D^+ beam. The α peak is broader than the proton peak because of energy straggling in the film. This means that the film has a higher stopping power for α particles then for protons. Nitrogen's nuclear reactions with the D beam are shown in the figures. The peak shown was the most prominent nuclear reaction, but there was a small satellite peak to the right of the main peak which is also a ^{14}N reaction as well as a small peak to the right of the ^{16}O α peak. Not shown in these figures 1-4 is a ^{12}C peak to the immediate right of the ^{16}O α peak. All these peaks can be seen in figure 5. The initial spectra show that all the samples contain from 5-6 percent of C. However, the C concentration is almost non-existent after the first hour of baking. After the third hour of

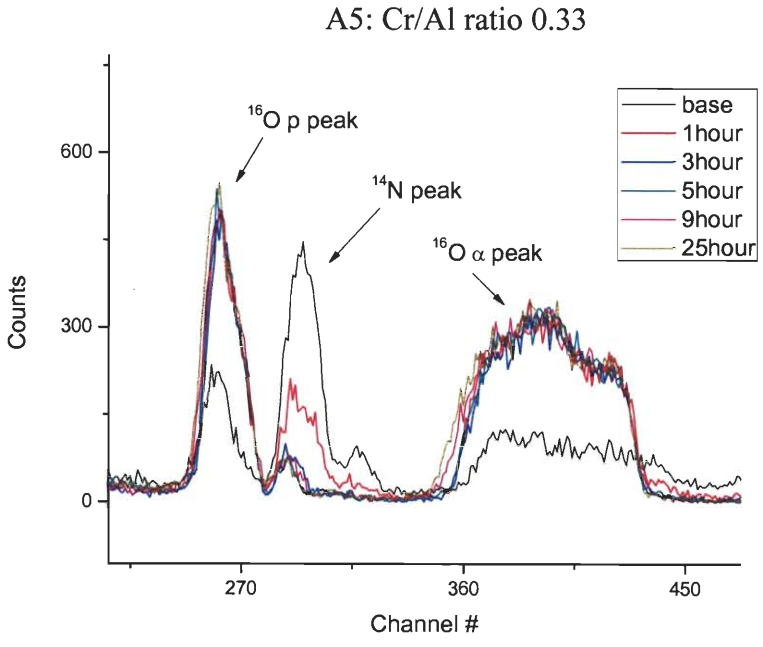

Fig. 1: Spectra of sample A5 taken with a 1.1 MeV D beam at 165 degree scattering angle.

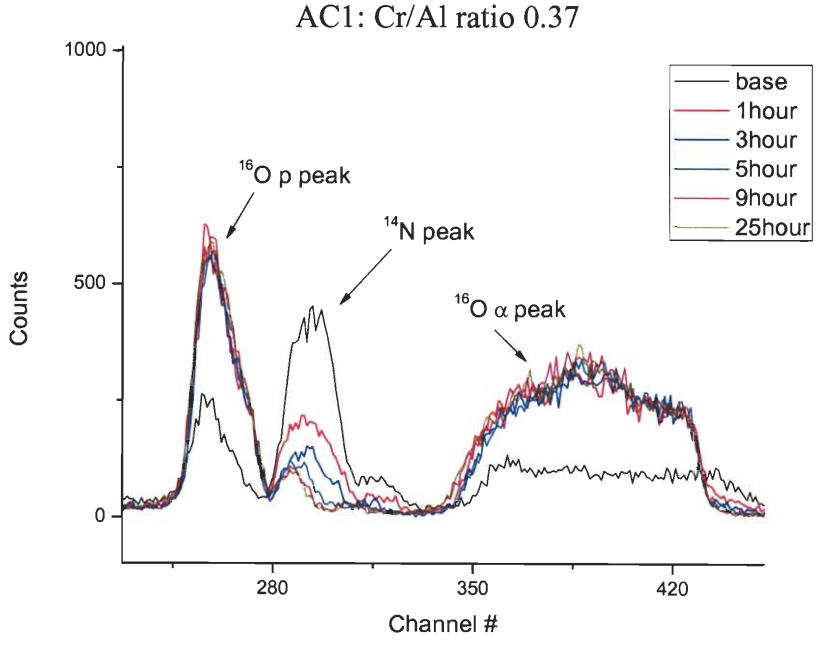

Fig. 2: Spectra of sample AC1 taken with a 1.1 MeV D beam at 165 degree scattering angle

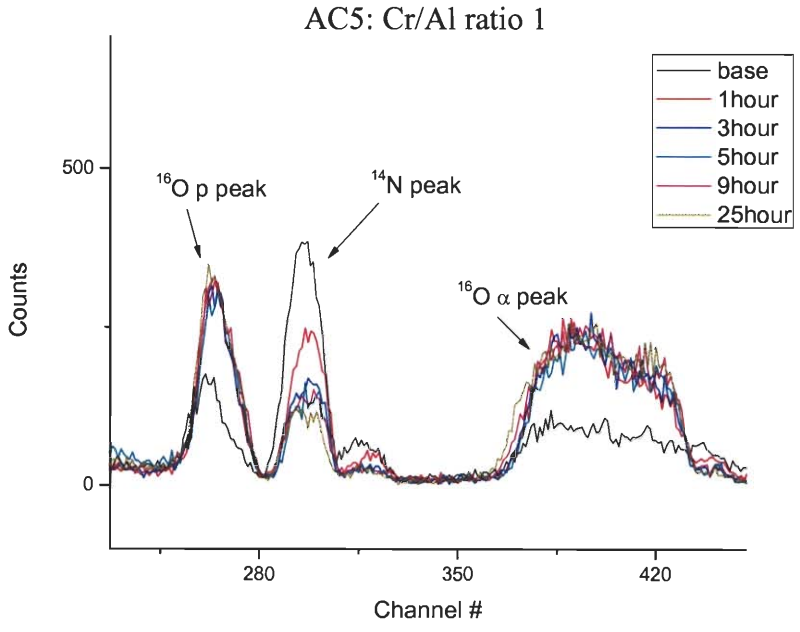

Fig. 3: Spectra of sample AC5 taken with a 1.1 MeV D beam at 165 degree scattering angle

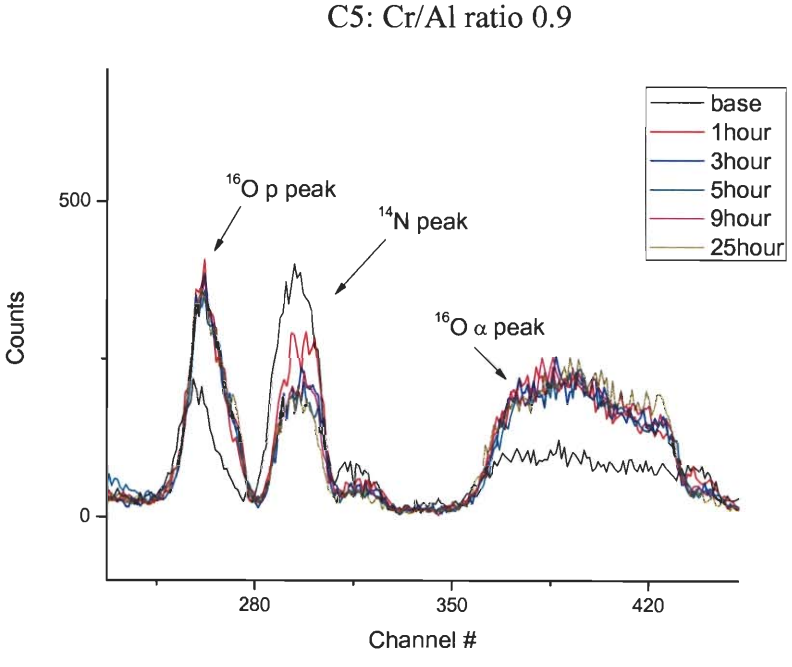

Fig. 4: Spectra of sample C5 taken with a 1.1 MeV D beam at 165 degree scattering angle

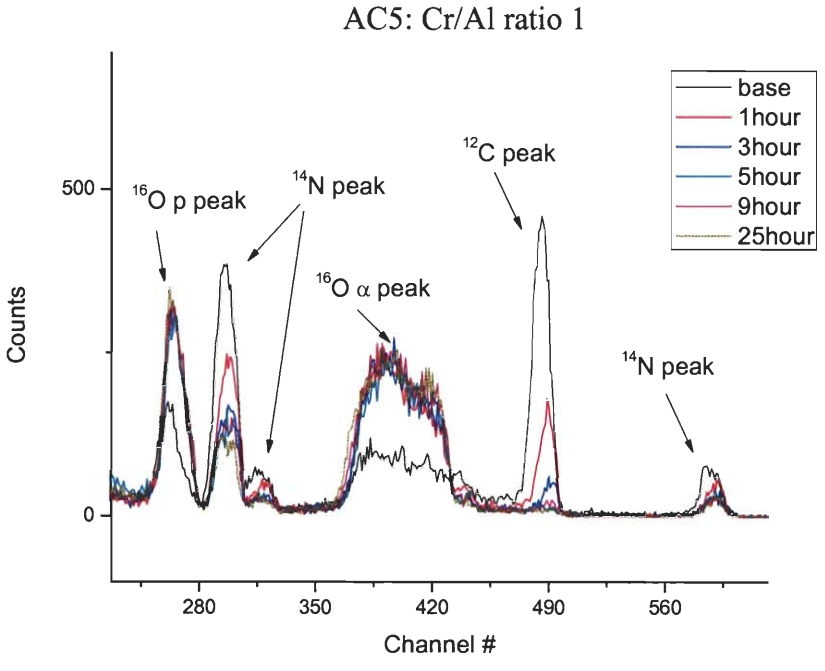

Fig. 5: All peaks shown for sample AC5 with a detector at 165 degrees and an incident beam of D^+

baking, only a trace amount of carbon is present for all the samples. This trace amount of carbon has been successfully modeled as being on the surface. Since we used carbon adhesive to place the samples on the sample holder, it is assumed that the trace amounts of carbon after the baking had occurred as a result of surface contamination, coming from the touch of our hand. Acetone and methanol were used to clean the surface of the samples upon realization, but some trace amounts still existed. However, the initial spectra show that the carbon is not merely on the surface, but in the interior of the CrAlN film as well. It must have been placed there during the deposition process. Most probably, carbon could find its place in the grain boundaries and during the oxidation process is reacting to the oxygen and escaping the coating as gas.

Notice the N loss and O gain in each of the samples as the oxidation of the samples were carried out. In some cases there is a rapid decrease in N content following the initial one-hour heat treatment, which is attributed to the transformation of CrN to Cr_2N [14,15]. It is further attribute a more gradual loss of N during subsequent annealing to the transformation of Cr_2N to Cr_2O_3. Formation of Cr_2O_3 could have formed a barrier layer for the subsequent oxygen to defuse into the sample. Moreover, is Cr_2O_3 is semiconductor, which will provide the conductivity required for the SOFC interconnect application. One of the desirable characteristics we wished to find is that some nitrogen is retained by the coating after the oxidation process, which indicates improved oxidation resistance. The final thickness of these coatings increases with the oxidation process because of the transformation of AlN to Al_2O_3 and CrN to Cr_2O_3. We expect AlN and

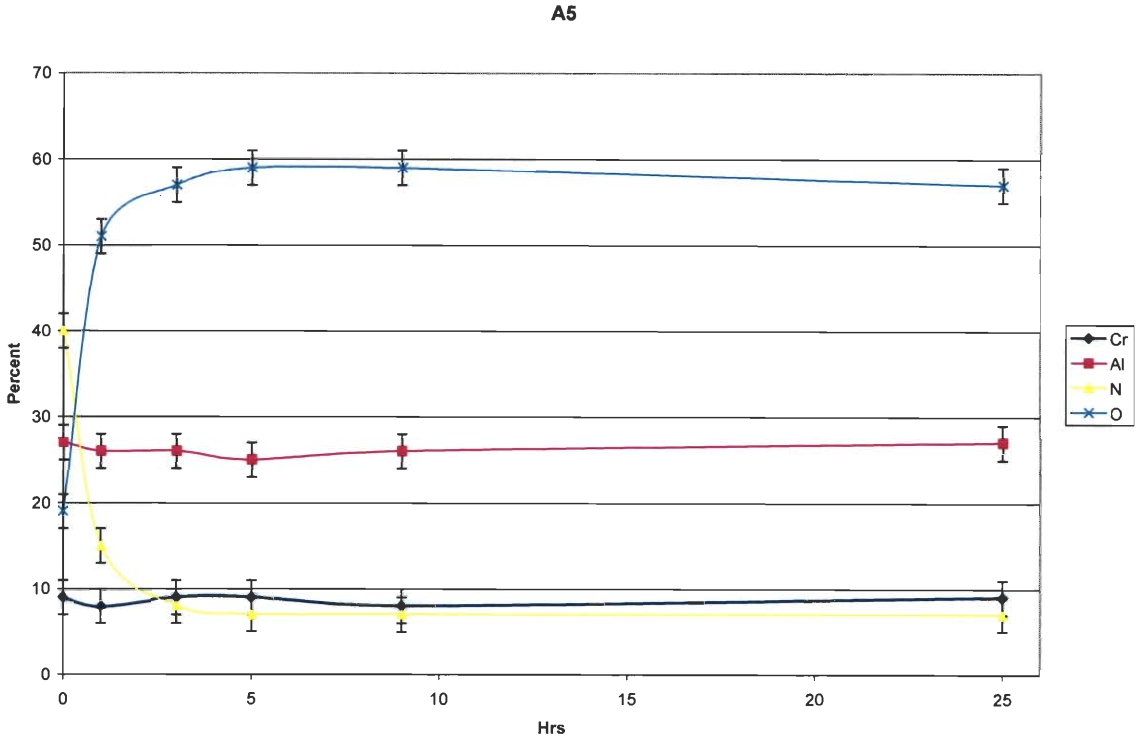

Fig. 6: Concentrations for sample A5. Percent composition is plotted against hours baked at 800 °C

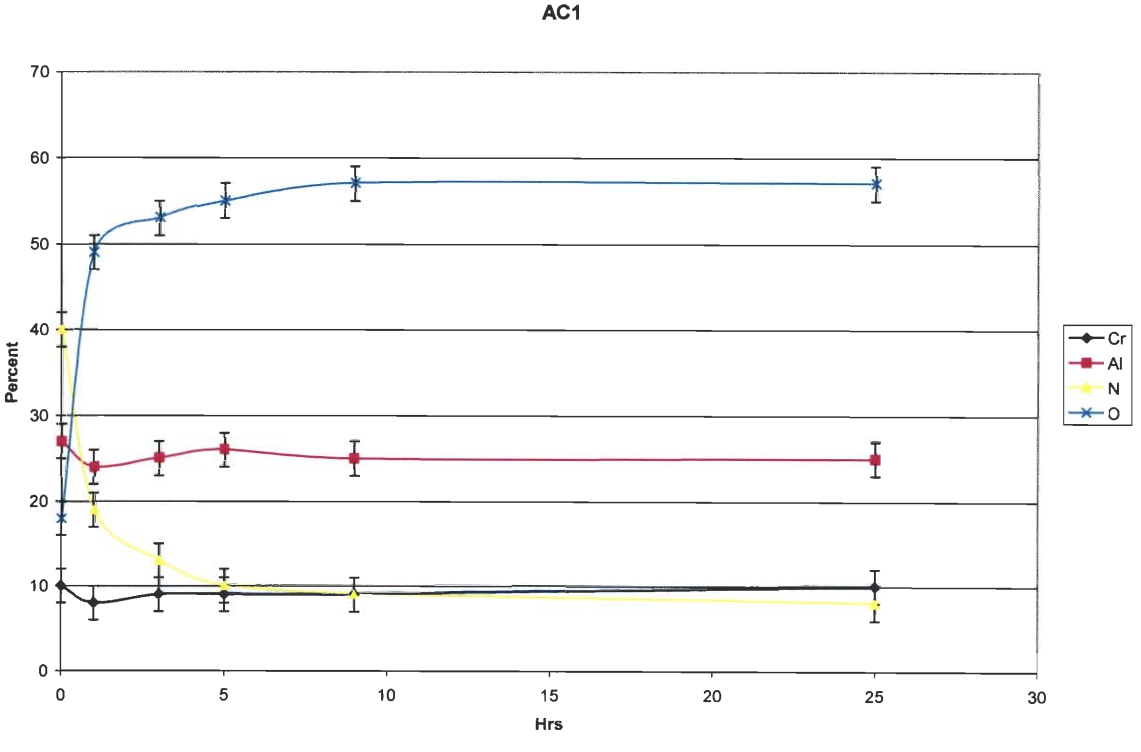

Fig. 7: Concentrations for sample AC1. Percent composition is plotted against hours baked at 800 °C

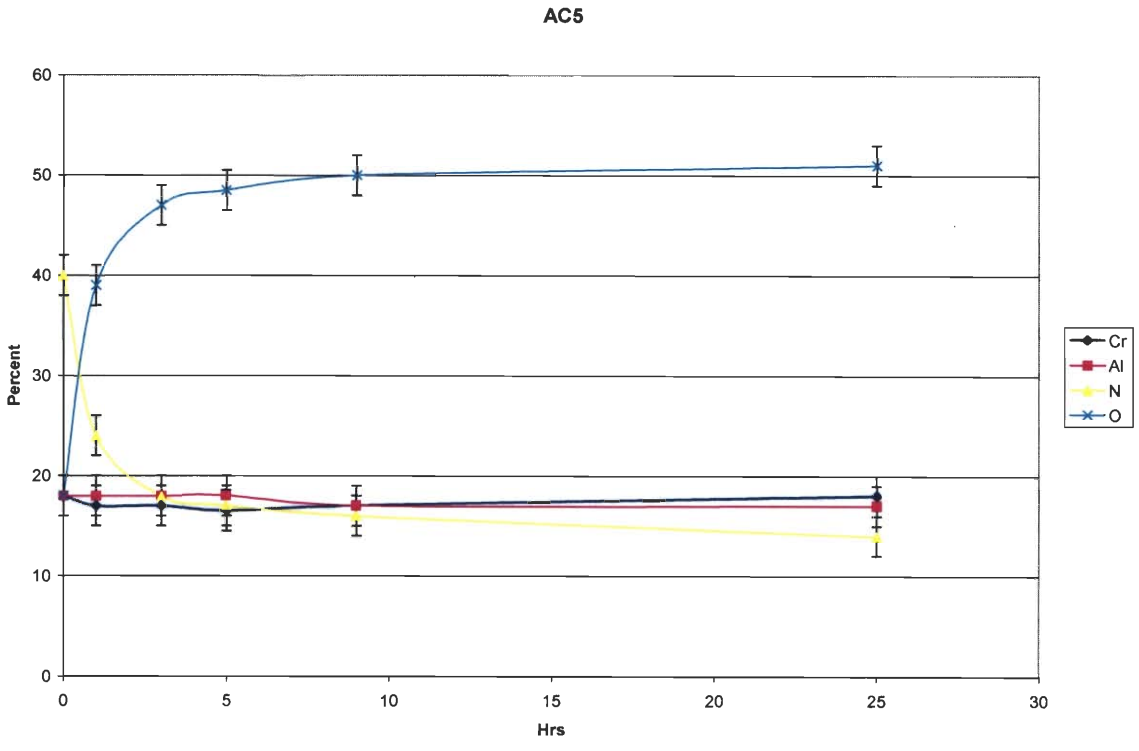

Fig. 8: Concentrations for sample AC5. Percent composition is plotted against hours baked at 800 °C

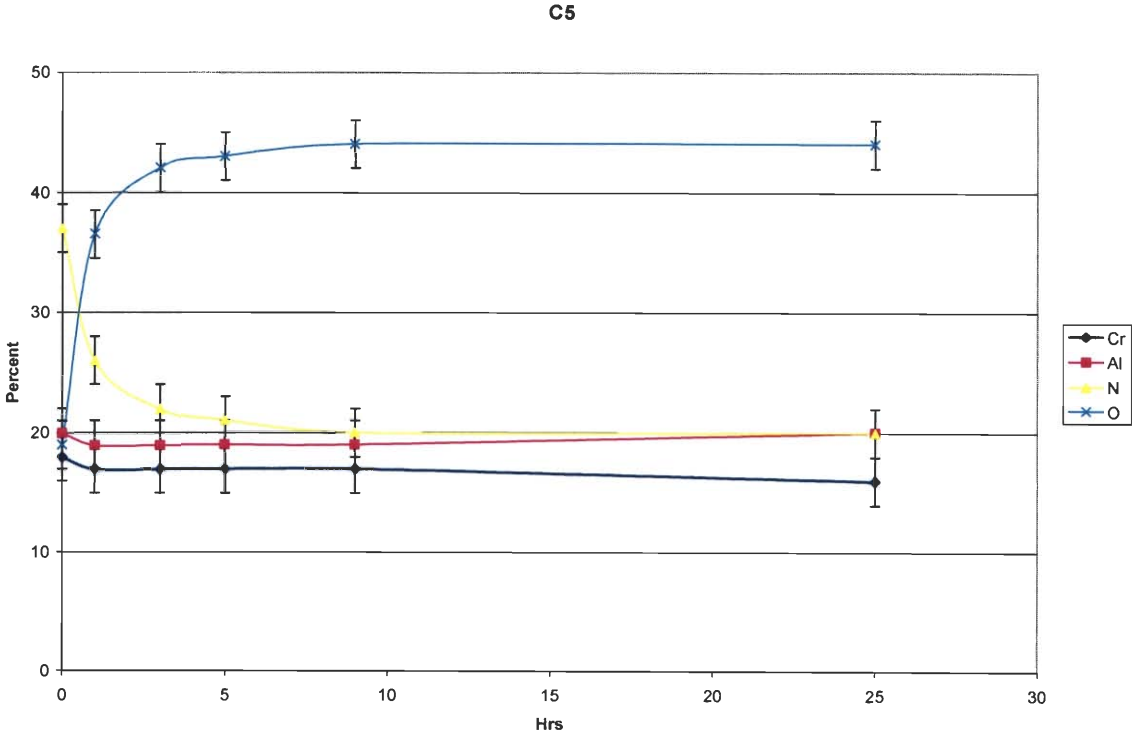

Fig. 9: Concentrations for sample C5. Percent composition is plotted against hours baked at 800 °C

CrN to be the dominant compounds present in as deposited coatings. However it has been reported that a stable fcc ternary phase with 71% aluminum in CrAlN exists [16]. Therefore, we expect stable ternary phase of CrAlN might exist in as deposited, Al rich coatings. Using the SIMNRA program to simulate the proton and deuteron spectra the concentrations in figures 5-9 were measured.

All of the samples followed the same trend. N loss and O gain in the first 5 hours followed by relative stability. The sample that performed the worst was A5. AC1 had a similar Cr/Al ratio as A5 and performed similarly. AC5 had the highest Cr/Al ratio, but performed poorer than C5 which had a slightly lower Cr/Al ratio. The low Cr/Al ratio samples performed poorly, while the high Cr/Al ratio samples were mixed. The sample that performed the best was C5 with a Cr/Al ratio of 0.9 which correlates an earlier study by Kayani et al.

Of particular interest in the previous figures is the initial O concentration in the samples. We had believed that we were studying CrAlN systems, when in fact we were studying CrAlON films. This initial O content is not likely caused by oxidation at room temperature but by presence of O during the sputtering process. This is a result that previous published results did not find. A 1.1 MeV D beam was not used in the previous study due to physical limitations.

Also of interest, substrate diffusion of a heavy element was noticed in the D spectra after several hours of baking for all samples. However, this was not studied due to technical

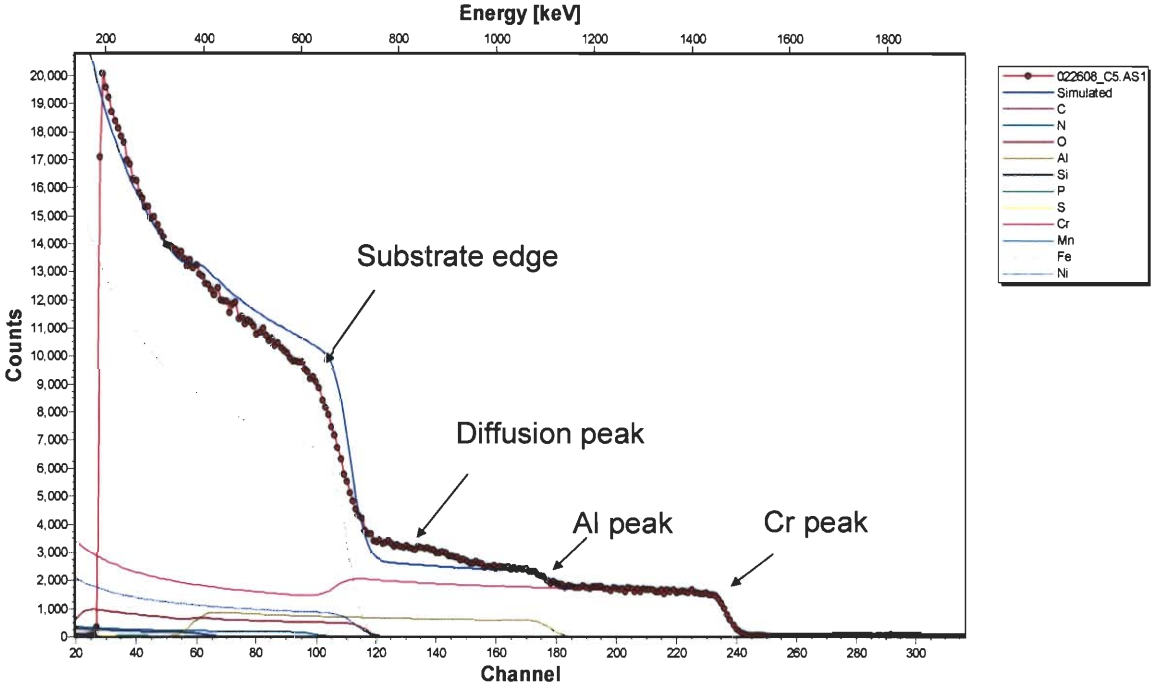

Fig. 10: He^{++} spectra of C5 taken after baking for 25 hours at 165 degree scattering angle. The blue line is the simulated spectra with no diffusion. The diffusion of the substrate blurs the substrate edge and causes a secondary peak.

difficulties in obtaining a ^4He beam. Such a beam would be needed for depth profiling the diffusion process. $^4He^{++}$ has a higher stopping power than D^+ and as a result has better depth resolution (due to more energy being lost in the same thickness of the sample leading to larger separation of peaks in the spectra). However, this diffusion can be clearly seen in ^4He spectra taken after the baking process in figure 10 when the technical difficulties were resolved.

The concentrations of the elements in the film have an estimated error of 2 %. This is due to the lack of a unique set of parameters that would model the spectra accurately. This could be improved for future work if the particles*sr was held constant. It appears that the sample was not held in a fixed position from one characterization to the next but rather moved with respect to the detector. This movement was very slight and could have been caused by jostling the experimental apparatus. Also, a slight electronic drift was noticed in the amplifier since the calibration factor changed by a small amount during the experiment. Both of these effects can be seen in figure 11.

We have shown a quantitative means of comparing the oxidation resistance of coated stainless steel samples. The results from ion beam analysis are quantitative and do not depend on the oxide stoichiometry which might change with depth. From our results, we conclude that Al rich coatings are more susceptible to oxidation than Cr rich coatings. We report early results for the high-temperature oxidation resistance of 430 stainless steel alloy with a coating of different Cr/Al ratios in an attempt to find the best ratio that is oxidation resistant. The best oxidation performance was demonstrated by sample C5 which has a Cr/Al ratio of 0.9. In subsequent studies, we intend to analyze the sample

coupons in the locations near that of sample coupon C5. Future measurements will extend the annealing time to better simulate the interconnect application in a solid oxide fuel cell as well as include resistivity measurements and depth profiling to study the substrate diffusion.

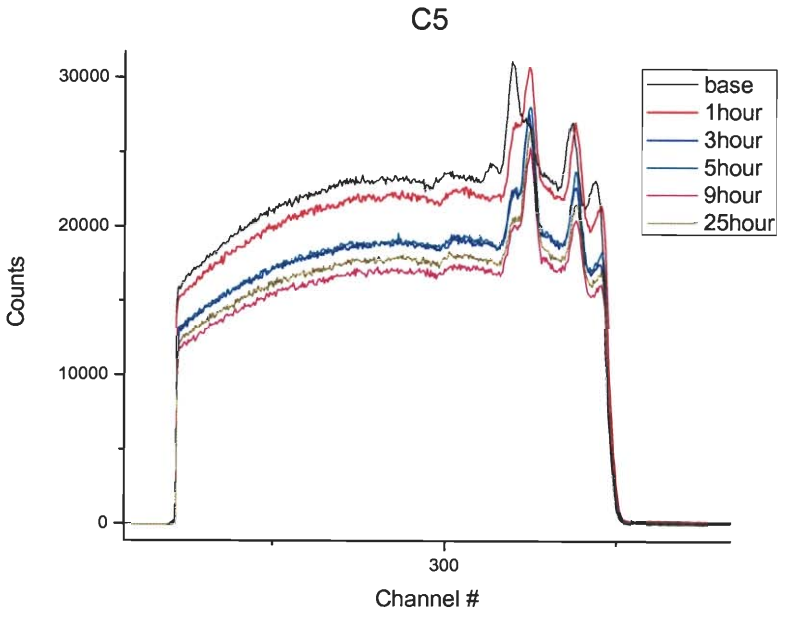

Fig. 11: H^+ spectra taken at 165 degrees scattering angle. Notice the change in the height of the spectra, this is due to the changing particles*sr. The shift in the peaks is due to a change in the calibration factor.

Reference:

1. Pointon K.D. (1997) "*Review of Work on Internal Reforming in the Solid Oxide Fuel Cell* ," ETSUreport F/01/00121/REP, AEA Technology, Harwell UK.

2 http://members.aol.com/profchm/t_table.html

3 Solid-oxide fuel cells (SOFC) with hydrocarbon and hydrocarbon-derived fuels Robert Kee, Huayang Zhu, and David Goodwin

4 http://www.science.uwaterloo.ca/~cchieh/cact/c123/nernsteq.html

5 http://www.sciencedirect.com/science?_ob=ArticleURL&_udi=B6TG0-40N7DBV-H&_use...

6. B.C.H. Steele and A. Heinzel, *"Materials for fuel-cell technologies"* Nature, 414 (2001) 345.

7. Z. Yang, K. S. weil, D.M. Paxton, and J.W. Stevenson: "*Selection and Evaluation of Heat-Resistant Alloys for SOFC Interconnect Applications"* J. Electrochem. Soc., 150 (2003) A1188.

8 J.R. Tesmer, M. Nastasi, Handbook of Modern Ion Beam Materials Analysis, Materials Research Society, Pittsburgh, PA, 1995.

9 M. Kawate, A.K. Hashimoto, and T. Suzuki, Surface and Coatings Technology, 165 (2003) 163-167.

10 O. Banakh, P.E. schmid, R. Sanjines, and F. Levy, Surface and Coatings Technology, 163-164, (2003) 57-61.

11 S. PalDey and S.C. Deevi, Materials Science and Engineering, A342, (2003) 58-79.

12 A. Kayani, T.L. Buchanan, M. Kopczyk, C. Collins, J. Lucas, K. Lund, R. Hutchison, P.E. Gannon, M.C. Deibert, R.J. Smith, D.-S. Choi, V.I. Gorokhovsky Surface & Coatings Technology 201 (2006) 4460–4466.

13 M. Mayer, SIMNRA User's Guide, Technical Report IPP 9/113, Max-Planck-Institut fur Plasmaphysik, Garching, Germany, 1997.

14 K. Huang, P.Y. Hou, and J.B. Goodenough, Materials Research Bulletin, 36 (2001) 81-95

15 H.-Y. Chen and F.-H. Lu, J. Vac. Sci. Technol. A, 21(3) (2003) 695-700

16 A.E. Reiter, T, V.H. Derflinger, B. Hanselmann, T. Bachmann, B. Sartory, Surface and Coatings Technology, 2114-2122 (2005) 200